

Differentiation of solitary brain metastasis from glioblastoma multiforme: a predictive multiparametric approach using combined MR diffusion and perfusion

Adam Herman Bauer¹ · William Erly² · Franklin G. Moser¹ · Marcel Maya¹ · Kambiz Nael²

Received: 29 December 2014 / Accepted: 24 March 2015 / Published online: 7 April 2015
© Springer-Verlag Berlin Heidelberg 2015

Abstract

Introduction Solitary brain metastasis (MET) and glioblastoma multiforme (GBM) can appear similar on conventional MRI. The purpose of this study was to identify magnetic resonance (MR) perfusion and diffusion-weighted biomarkers that can differentiate MET from GBM.

Methods In this retrospective study, patients were included if they met the following criteria: underwent resection of a solitary enhancing brain tumor and had preoperative 3.0 T MRI encompassing diffusion tensor imaging (DTI), dynamic contrast-enhanced (DCE), and dynamic susceptibility contrast (DSC) perfusion. Using co-registered images, voxel-based fractional anisotropy (FA), mean diffusivity (MD), K^{trans} , and relative cerebral blood volume (rCBV) values were obtained in the enhancing tumor and non-enhancing peritumoral T2 hyperintense region (NET2). Data were analyzed by logistic regression and analysis of variance. Receiver operating characteristic (ROC) analysis was performed to determine the optimal parameter/s and threshold for predicting of GBM vs. MET.

Results Twenty-three patients (14 M, age 32–78 years old) met our inclusion criteria. Pathology revealed 13 GBMs and 10 METs. In the enhancing tumor, rCBV, K^{trans} , and FA were higher in GBM, whereas MD was lower, neither without statistical significance. In the NET2, rCBV was significantly

higher ($p=0.05$) in GBM, but MD was significantly lower ($p<0.01$) in GBM. FA and K^{trans} were higher in GBM, though not reaching significance. The best discriminative power was obtained in NET2 from a combination of rCBV, FA, and MD, resulting in an area under the curve (AUC) of 0.98.

Conclusion The combination of MR diffusion and perfusion matrices in NET2 can help differentiate GBM over solitary MET with diagnostic accuracy of 98 %.

Keywords Glioblastoma multiforme · Intracranial metastasis · Dynamic contrast enhancement · Dynamic susceptibility contrast · Diffusion tensor imaging

Introduction

Glioblastoma multiforme (GBM) comprises about 40–50 % of all primary malignant brain tumors in adults [1], and brain metastases occur in 10–30 % of adults, with approximately 50 % seemingly solitary at diagnosis [2]. History of a primary malignancy, multiplicity of lesions, location at the gray-white junction, and non-infiltrating appearance are characteristics traditionally utilized to help differentiate metastasis (MET) from GBM. Nonetheless, primary brain malignancies can present in patients with systemic cancer and solitary intracranial brain MET can be the first manifestation of extracranial malignancy. Brain MET and GBM can appear similar on conventional MRI, and therefore, reliable imaging differentiation between MET and GBM can be important for medical staging, surgical planning, and therapeutic decision making [3–5].

Acknowledging its importance, many investigators have used morphological features and advanced MRI techniques such as magnetic resonance (MR) diffusion and perfusion to differentiate GBM from MET. Feature extraction and

✉ Adam Herman Bauer
adam.herman.bauer@gmail.com

¹ Department of Medical Imaging, Cedars-Sinai Medical Center, 8700 Beverly Blvd., Taper Bldg., Suite M335, Los Angeles, CA 90048, USA

² Department of Medical Imaging, University of Arizona Medical Center, Tucson, AZ, USA

segmentation algorithms have been demonstrated as favorable techniques to distinguish GBM from MET [6, 7]. Diffusion tensor imaging (DTI) has been applied for differentiating GBM from MET with mixed results [8–12]. Recent data from Wang et al. have shown DTI to be a very promising imaging tool to differentiate GBM from MET [8, 9]. Other investigators have used MR perfusion to differentiate solitary MET from GBM either by taking advantage of the existing differences in hemodynamic curve analysis and utilizing the parameters of peak height and percentage signal recovery [4] or by using dynamic susceptibility contrast (DSC)-derived relative cerebral blood volume (rCBV) to exploit the differences in tumor vascularity and angiogenesis between the two [13, 14]. More recently, researchers have investigated the differences between GBM and MET utilizing a combination of these techniques [15, 16].

The purpose of this study was to use a combination of MR diffusion (DTI-fractional anisotropy (FA) and mean diffusivity (MD)) and MR perfusion (DSC-relative cerebral blood volume (rCBV) and dynamic contrast-enhanced (DCE)- K^{trans}) parameters to create a predictive multiparametric imaging approach that can be used to differentiate MET from HG in patients with solitary enhancing brain mass.

Methods

Patients

This retrospective single-institutional study was conducted between 24 June 2013 and 10 June 2014. All examinations were performed in accordance with institutional review board guidelines with an approved study protocol. Inclusion criteria were as follows: (1) patients with single solitary enhancing brain mass with clinical question of MET vs. GBM; (2) pretreatment acquisition of 3.0 T MRI brain tumor protocol including DSC, DCE, and DTI; and (3) confirmed surgical pathology.

Image acquisition

All patients underwent MRI on a 3.0 T Siemens Skyra MRI system (Siemens; Erlangen, Germany). The imaging protocol included transverse T1WI (TR/TE/FA 600/82 ms/180°), T2WI (TR/TE/FA 7000/100 ms/180°), FLAIR (TR/TE/TI 9000/81/2500 ms), gradient recalled echo (TR/TE/FA 870/20 ms/20°), DTI, DCE, and DSC perfusion imaging.

DTI was acquired using single-shot spin-echo EPI (TR/TE, 5500/82 ms; FOV 22 cm×22 cm; matrix 128 mm; slices 40×3 mm, voxel size 1.5×1.5×3 mm). Diffusion gradients were applied along 20 noncollinear directions with a b value of 1000 s/mm² resulting in a 6-min acquisition time. A generalized partial parallel acquisition (GRAPPA) [17] technique with acceleration factor of 3 was used.

The DCE perfusion was accomplished by using a 3D radial volumetric interpolated examination (VIBE) sequence (TR/TE (ms) 3.6/1.7, FA 120, voxel size 1.4×1.4×3 mm). A total of 328 radial views were acquired in eight rotations (42 views/rotation) with “stack-of-stars” scheme: i.e., normal sampling in the z-direction and radial sampling in the xy-plane. Three measurements were obtained each divided into eight subframes by applying K-space weighted image contrast echo-sharing [18], resulting in 3-min acquisition time with a 4-s temporal resolution. Varying flip angle methodology with flip angles of 2°, 5°, 9°, and 15° was implemented for the generation of T1 maps [19].

DSC perfusion was performed using a single-shot gradient-echo EPI sequence with the following parameters: TR/TE 1450/22 ms, FA=90°, FOV 22 cm×22 cm, matrix 128×128 mm, 30×4 mm slices, GRAPPA=3, and 60 dynamic frames.

A total volume of 0.15 mmol/kg of Gd-DTPA was used to accomplish both DCE and DSC perfusion imaging. First, 40 % of contrast volume was injected at 5 cc/s for DCE imaging. This injection was considered as a preload to rectify leakage correction for subsequent DSC imaging [20]. There was an 8-min interval gap between DCE and DSC in which axial T2 and T1 postcontrast images were obtained. Subsequently, the remaining 60 % of contrast solution was injected at 5 ml/s for the DSC perfusion scan. All injections were performed using an electronic power injector via 18-gauge antecubital venous access. Each contrast injection was flushed with 20 ml of normal saline.

Image analysis

MR perfusion and DTI studies were processed using commercially available FDA-approved software (Olea Sphere, Olea Medical SAS, La Ciotat, France). The arterial input function was selected automatically and multiparametric perfusion maps were calculated using an extended toft model [21] for DCE and block-circulant singular value decomposition technique [22] for DSC. The rCBV and K^{trans} maps derived from DSC and DCE perfusion datasets, respectively, were then exported from the software for subsequent analysis. DTI analysis was also performed by the Olea DTI package where FA and mean diffusivity (MD) maps were calculated using standard methods [23].

The FLAIR and T1WI-postcontrast images, CBV, K^{trans} , MD, and FA maps for each patient were coregistered by the OleaSphere software using a 6-degree of freedom transformation and a mutual information cost function. This was followed by visual inspection to ensure adequate alignment.

Then, regions of interest were drawn manually on enhancing tumor and NET2 using coregistered images. The NET2 was defined as the T2 hyperintense region on FLAIR images within 2 cm around the enhancing tumor. Depending on the

size of the tumor, this was performed on two to three slices for each patient with average region of interest volumes of 1656 (± 1202) and 2103 (± 1445) mm³ for enhancing and NET2 regions, respectively. rCBV, K^{trans} , FA, and MD values for each voxel in the enhancing tumor and NET2 were calculated and exported into an excel spreadsheet for statistical analysis.

Statistical analysis

Univariate analysis of variance was performed for rCBV, FA, MD, and K^{trans} between GBM and MET in the enhancing and NET2 regions. Multivariate ANOVA was then performed for each parameter to assess overall differences between regions (enhancing tumor and NET2) in addition to GBM and MET. $P < 0.05$ was considered to indicate a statistically significant difference. Receiver operating characteristic (ROC) analysis was performed to determine the optimal parameter(s) (rCBV, K^{trans} , FA, MD) in distinguishing MET from GBM in both enhancing tumor and NET2. Optimal thresholds were calculated for each ROC curve to maximize both sensitivity and specificity employing the Youden statistic. Subsequently, a combined ROC curve for combination of parameters was calculated extrapolating from the maximum likelihood estimation model of combining classifiers [24]. Area under the curve was calculated for each individual classifier's ROC curve as well as for the combined ROC curves.

Results

Twenty-three patients (14 M, 9 F, age 32–78 years old) met our inclusion criteria. Thirteen patients had histologically confirmed GBM. Ten patients had surgically proven brain MET: non-small cell lung adenocarcinoma ($n=4$), colon adenocarcinoma ($n=1$), breast adenocarcinoma ($n=2$), melanoma ($n=1$), ovarian serous adenocarcinoma ($n=1$), and neuroendocrine tumor ($n=1$).

The quantitative values including mean \pm SD and corresponding statistical analysis of rCBV, FA, MD, and K^{trans} in the enhancing tumor and NET2 for both GBM and MET are

summarized in Table 1. Figure 1 shows an example of our multiparametric MRI in a patient with GBM.

For enhancing regions, the rCBV, K^{trans} , and FA were higher in GBM, whereas MD was lower in GBM, neither demonstrating statistical significance (Table 1). For NET2 regions, the rCBV was significantly ($p=0.05$) higher in GBM, while MD was significantly ($p < 0.01$) lower in GBM (Table 1). Multivariate analysis resulted in statistically significant differences in means ($p < 0.05$) between the enhancing and NET2 regions for rCBV, FA, MD, and K^{trans} . ROC curve analysis results are exhibited in Fig. 2. For each parameter, area under the curve (AUC) and threshold values with their associated sensitivity and specificity are listed in Table 2.

For the enhancing tumor, the discriminative power of our individual imaging biomarkers was highest for FA with an AUC of 0.87. The best diagnostic accuracy in the enhancing tumor was obtained by combining rCBV and FA with resultant AUC of 0.94 compared to either parameter alone (0.68 and 0.87). In the enhancing tumor, using rCBV > 1.96 and FA > 0.13 , GBM could be differentiated from MET with sensitivity and specificity of 88 and 85 %. For the NET2, the discriminative power of our individual imaging biomarkers was comparable with the highest AUC of 0.83 for MD. The best discriminative power in NET2 was achieved by combination of rCBV, FA, and MD with an AUC of 0.98. In the NET2, using rCBV > 3.14 , FA > 0.22 , and MD $< 143 \times 10^{-6}$ mm² s⁻¹, GBM could be differentiated from MET with sensitivity and specificity of 90 and 100 %.

Subanalysis of metastatic lesions showed no significant difference in rCBV, K^{trans} , FA, or MD between the four cases of adenocarcinoma and the remaining metastases in both the enhancing tumor and NET2.

Discussion

Our study showed that there are differences in MR perfusion and diffusion biomarkers between MET and GBM that can be exploited to differentiate solitary MET from GBM. The ROC analysis indicated that the best overall model to distinguish GBM from MET is a combination of rCBV, FA, and ADC in

Table 1 Multivariate analysis for the differentiation of GBM and MET using mean rCBV, FA, MD, and K^{trans} in enhancing and NET2 regions

Parameter	Region	Glioma (mean)	SD	Mets (mean)	SD	<i>p</i> value	ANOVA <i>p</i> value
rCBV	Enhancing tumor	3.87	1.17	2.55	1.20	0.10	0.01
	NET2	1.71	1.21	0.94	1.25	0.05	
FA	Enhancing tumor	0.23	0.04	0.11	0.05	0.09	0.02
	NET2	0.27	0.05	0.16	0.05	0.10	
MD ($\times 10^{-6}$ mm ² s ⁻¹)	Enhancing tumor	119.07	10.28	133.28	12.05	0.38	0.02
	NET2	110.49	6.84	145.13	8.03	0.004	
K^{trans} (min ⁻¹)	Enhancing tumor	0.43	0.14	0.18	0.16	0.26	0.21
	NET2	0.10	0.04	0.06	0.05	0.57	

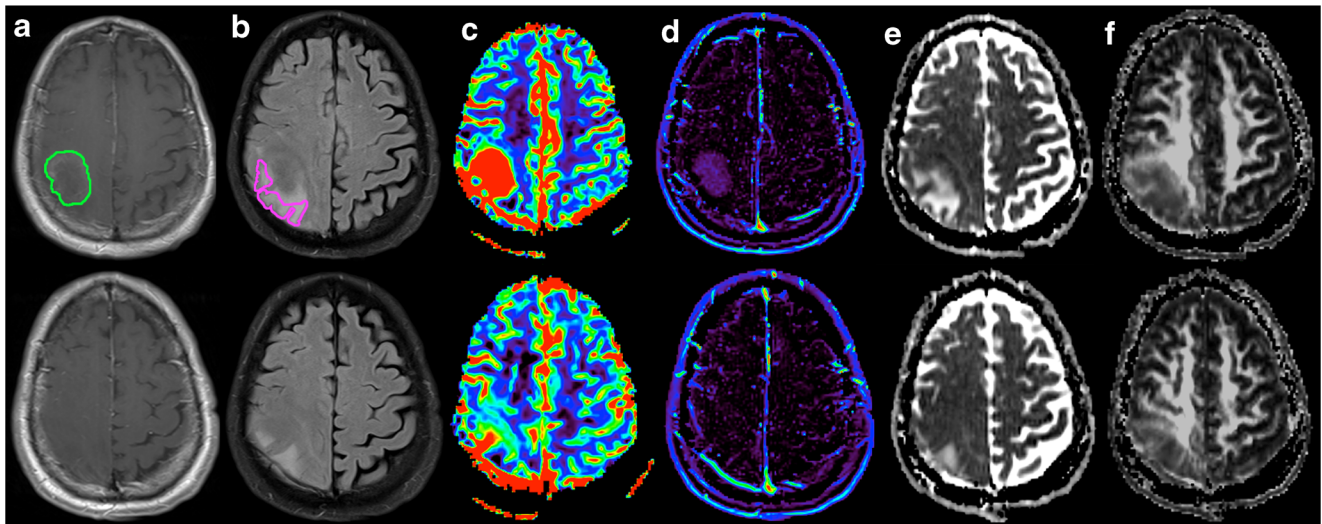


Fig. 1 Pretreatment contrast-enhanced T1 (a), FLAIR (b), DSC-rCBV (c), DCE- K^{trans} (d), MD (e), and FA (f) maps in a 74-year-old woman subsequently diagnosed as having GBM. *Upper row*: in the enhancing region, there is significant increase in rCBV (6.9) and K^{trans} (0.22 min^{-1}). The values of MD and FA are $915 \times 10^{-6} \text{ mm}^2 \text{ s}^{-1}$ and 0.25, respectively.

Example regions of interest are provided for this slice around the enhancing and NET2 components. *Lower row*: in NET2, there is also significant increase in rCBV (3.2) but normal K^{trans} (0.04 min^{-1}). The mean values of diffusion parameters are lower in NET2 in comparison to enhancing tumor with $715 \times 10^{-6} \text{ mm}^2 \text{ s}^{-1}$ and 0.12 for MD and FA, respectively

NET2 with an AUC of 0.98 superior to any individual or combination of other classifiers. In the enhancing regions of tumor, the best discriminative power was achieved by using rCBV and FA with resultant AUC of 0.94.

In distinguishing GBM from solitary MET using the described imaging model, special attention should be given to NET2 rather than enhancing tumor. The enhancing area of both GBM and MET is heterogeneous often with architectural distortion, necrosis, hemorrhage, and vascular proliferation, all of which can distort the normal parenchymal microarchitecture including white matter tracts, capillary bed, and extracellular matrix [25, 26]. Conversely, the NET2

is more homogeneous where the absence of necrosis and hemorrhage preserves the microenvironmental structure. Our results reflect this histological contradistinction. We highlight two primary findings:

DSC-rCBV

We observed significantly higher rCBV values in GBM compared to those in MET in the NET2 and elevation of rCBV in the enhancing region in GBM concordant with prior reports in the literature [4, 13, 14]. Our results showed a moderate discriminative power for rCBV in differentiation of MET from

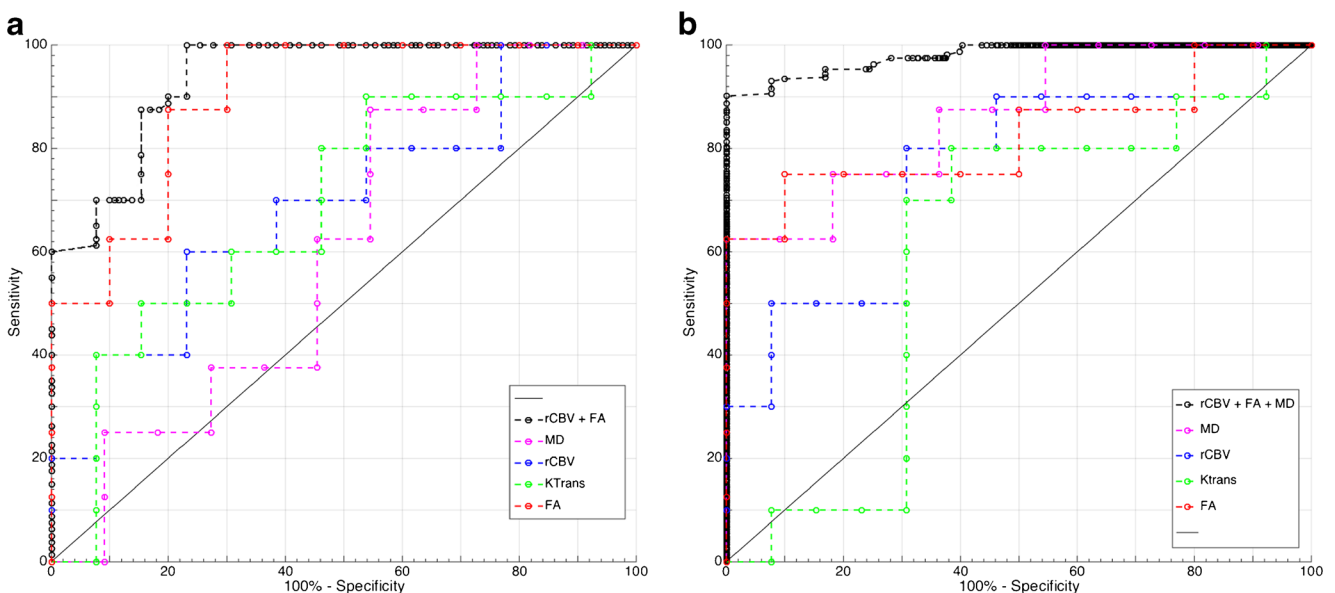


Fig. 2 ROC analysis with AUC for each imaging biomarker and best combined AUC for enhancing (a) and NET2 (b)

Table 2 ROC analysis of different imaging biomarkers in enhancing and NET2 regions between GBM and MET

Region	Classifier	Threshold values	Sensitivity (%)	Specificity (%)	Area under the curve
Enhancing tumor	rCBV	3.75	70	62	0.68
	FA	0.12	88	80	0.87
	MD	$143 \times 10^{-6} \text{ mm}^2 \text{ s}^{-1}$	63	55	0.57
	K^{trans}	0.3 min^{-1}	60	69	0.68
	rCBV+FA	1.96/0.13	88	85	0.94
NET2	rCBV	1.56	80	69	0.74
	FA	0.2	75	90	0.82
	MD	$132 \times 10^{-6} \text{ mm}^2 \text{ s}^{-1}$	75	82	0.83
	K^{trans}	0.034 min^{-1}	70	69	0.59
	rCBV+FA+MD	3.14, 0.22, $143 \times 10^{-6} \text{ mm}^2 \text{ s}^{-1}$	90	100	0.98
	rCBV+FA	3.14, 0.20	83	90	0.93
	rCBV+MD	2.2, $143.3 \times 10^{-6} \text{ mm}^2 \text{ s}^{-1}$	81	92	0.93
FA+MD	0.2, $143.3 \times 10^{-6} \text{ mm}^2 \text{ s}^{-1}$	91	90	0.96	

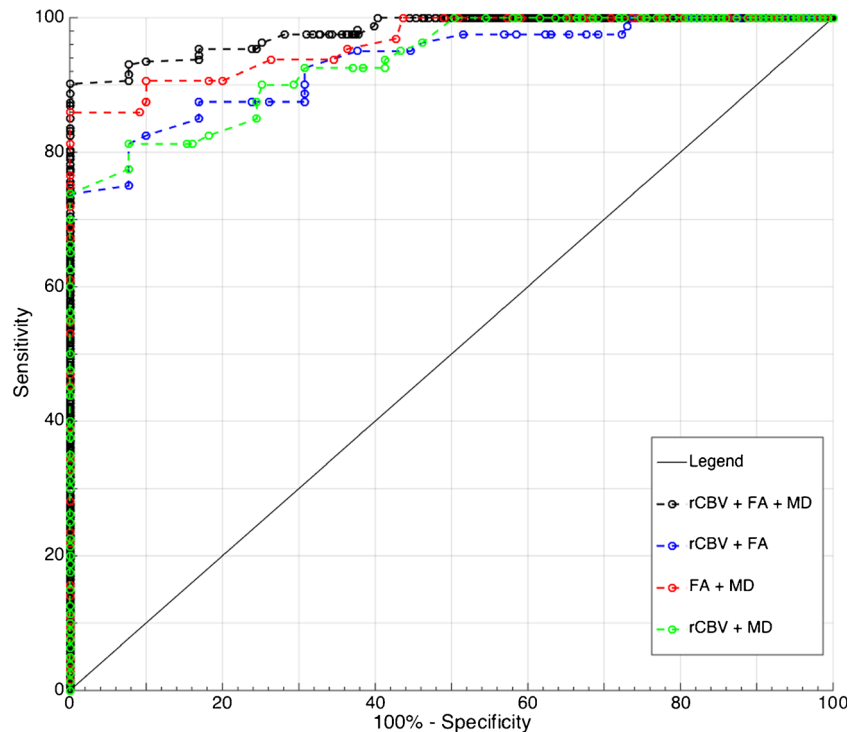
GBM with AUC of 0.68 and 0.74 for enhancing and NET2, respectively. As shown by others [27, 28], our results suggest that rCBV alone may be less than ideal for differentiating MET from GBM, particularly in the enhancing region in which we found lower AUC, and less sensitivity/specificity to differentiate MET from GBM. This may be explained by the fact that angiogenesis, although a feature of GBM [25], is also present in many hematogenous brain metastases. rCBV as a biomarker of increased angiogenesis should therefore be interpreted with caution in differentiating MET from GBM, particularly within enhancing tumor. On the other hand, improved performance of rCBV in NET2 compared to within enhancing tumor as shown

in our study and others [4, 13, 14] likely relies on the discongruity of tissue composition between MET and GBM, where neoangiogenesis and increased neoplastic cellularity are widespread within GBM-NET2 while vasogenic edema dominates the MET-NET2 [26].

DTI

As shown in several prior reports [9, 29], we found higher FA and lower MD in both enhancing and NET2 of GBM compared to those of MET. Our results in particular showed that while FA has better discriminatory power in the enhancing

Fig. 3 ROC analysis with AUC for combinations of imaging biomarkers in the NET2



tumor, MD has better diagnostic accuracy in NET2 compared to enhancing region concordant with other reports [30]. Within the enhancing region, higher FA and lower MD in GBM compared to those of MET resulted in AUC of 0.87 and 0.57, respectively. The diagnostic performance was comparable in NET2, where higher FA and lower MD in GBM resulted in AUC of 0.82 and 0.83, respectively.

Changes in diffusion biomarkers are explained by underlying brain microstructure and histology [31]. Lower MD, an indication of higher cellularity, and higher FA, an indication of increased anisotropy along the WM tracts and structured orientation, can be seen in GBM [9, 32].

Although there is agreement on the beneficial role of MR diffusion for differentiation of MET vs. GBM, there are discrepant reports as to which region of the tumor these biomarkers should be applied and how to define those regions. Our results showed better discriminative power in NET2 for MD and the combination of FA and MD as suggested by a prior report [30, 33]. There are however reports of heterogeneity of diffusion data in NET2 [34] or even better diagnostic performance in enhancing tumor [9, 29]. Along these lines, FA individually performed better within the enhancing tumor. The discrepancies between these studies including FA and MD values may be not only due to differences in the underlying histology of tumor but also secondary to varying degrees of tumor heterogeneity in the enhancing region due to necrosis, calcification, and hemorrhage.

The finding that K^{trans} was essentially noncontributory was unexpected. While DSC measures the angiogenesis and vascular proliferation, K^{trans} provides a measure of microvascular permeability. In the heterogeneous and complex microenvironment of the tumor bed [35], K^{trans} depends not only on vascular permeability but also on a combination of blood flow, vascular surface area, and hydrostatic and osmotic pressures [36]. Though not significant, our finding of increased K^{trans} in the enhancing portion of tumor regardless of being MET or GBM is an expected observation, since contrast enhancement indicates BBB breakdown and, hence, increase in permeability. Because K^{trans} is the product of vascular permeability and vascular surface area [37], one expects higher K^{trans} values in the enhancing region of GBM than K^{trans} values in the enhancing region of MET due to increased vascular surface area, as is shown in our results. The ROC analysis showed only modest discriminative power to differentiate MET from GBM with AUC of 0.68 and 0.59 for enhancing and NET2, respectively.

The combination of multiple parameters allows for increased diagnostic accuracy that is further improved with additional classifiers. This is analogous to the imaging diagnosis of meningioma. Alone, an enhancing mass is nonspecific. However, with an additional qualifier of dural-based, the probability of meningioma is increased. Furthermore, additional characteristics of homogeneous enhancement, the presence of a dural tail, and internal restricted diffusion dramatically

increase the probability that the enhancing mass is a meningioma. In a similar manner, the additional diagnostic information provided by each parameter can be combined to yield improved diagnostic performance. Our imaging approach allows for the quantification of this process, as demonstrated in the ROC curves of combinations of parameters within the NET2 (Fig. 3). A combination of two parameters (Fig. 3) results in diagnostic accuracy superior to a single parameter alone (Fig. 2), and a combination of three parameters gives additional diagnostic power. When utilizing the ROC of a combination of three parameters, there exists the possibility of disagreement between thresholds. In these cases of false positive (or false negative) values, the two-parameter ROC curves can be referenced to evaluate conflicting values.

Our study has several limitations. First, our small sample size is too small which limits the conclusion. The results of this study need to be confirmed in a larger clinical cohort. Second, the retrospective nature of the study can introduce unknown bias. For the same reason, we were unable to spatially match histology with our imaging biomarkers within a specific ROI. Third, we only included the two most common solitary enhancing lesions in our practice and did not include other possible solitary lesions such as cerebral abscesses or lymphoma. We thought that mixing other lesions could further dilute the statistical analysis of our study. Lastly, the heterogeneity of the metastatic origin in our study warrants consideration. Differing microvascular environments from various origins may inadvertently lead to increased variability in our results. Future studies with larger sample size and prospective approaches to enable direct correlation of imaging with histologic observations are warranted to further investigate the diagnostic potential of the presented imaging approach.

Conclusion

There is a significant difference in DTI (MD) and MR perfusion (rCBV) matrices between MET and GBM with better diagnostic performance in the NET2 than in the enhancing region. Using our multiparametric MRI, the best overall model to distinguish GBM from MET consisted of a combination of rCBV, FA, and ADC within the NET2 yielding an AUC of 0.98, superior to any individual or combination of other classifiers. The results of this study should be confirmed in a larger cohort.

Ethical standards and patient consent We declare that all human and animal studies have been approved by the University of Arizona IRB and have therefore been performed in accordance with the ethical standards laid down in the 1964 Declaration of Helsinki and its later amendments. We declare that all patients gave informed consent prior to inclusion in this study.

Conflict of interest KN consults for Olea Medical.

References

- Sherwood PR, Stommel M, Murman DL, Given CW, Given BA (2004) Primary malignant brain tumor incidence and medicaid enrollment. *Neurology* 62:1788–1793
- Ranjan T, Abrey LE (2009) Current management of metastatic brain disease. *Neurotherapeutics* 6:598–603
- Mukundan S, Holder C, Olson JJ (2008) Neuroradiological assessment of newly diagnosed glioblastoma. *J Neuro-Oncol* 89:259–269
- Cha S, Lupo JM, Chen MH, Lamborn KR, McDermott MW, Berger MS et al (2007) Differentiation of glioblastoma multiforme and single brain metastasis by peak height and percentage of signal intensity recovery derived from dynamic susceptibility-weighted contrast-enhanced perfusion mr imaging. *AJNR Am J Neuroradiol* 28:1078–1084
- Giese A, Westphal M (2001) Treatment of malignant glioma: a problem beyond the margins of resection. *J Cancer Res Clin Oncol* 127:217–225
- Yang G, Jones TL, Barrick TR, Howe FA (2014) Discrimination between glioblastoma multiforme and solitary metastasis using morphological features derived from the p:q tensor decomposition of diffusion tensor imaging. *NMR Biomed* 27(9):1103–1111
- Blanchet L, Krooshof PW, Postma GJ, Idema AJ, Goraj B, Heerschap A, Buydens LM (2011) Discrimination between metastasis and glioblastoma multiforme based on morphometric analysis of MR images. *AJNR Am J Neuroradiol* 32(1):67–73
- Wang S, Kim SJ, Poptani H, Woo JH, Mohan S, Jin R et al (2014) Diagnostic utility of diffusion tensor imaging in differentiating glioblastomas from brain metastases. *AJNR Am J Neuroradiol* 35:928–934
- Wang S, Kim S, Chawla S, Wolf RL, Zhang WG, O'Rourke DM et al (2009) Differentiation between glioblastomas and solitary brain metastases using diffusion tensor imaging. *NeuroImage* 44:653–660
- Mouthuy N, Cosnard G, Abarca-Quinones J, Michoux N (2012) Multiparametric magnetic resonance imaging to differentiate high-grade gliomas and brain metastases. *J Neuroradiol* 39(5):301–307
- Yamasaki F, Kurisu K, Satoh K, Arita K, Sugiyama K, Ohtaki M et al (2005) Apparent diffusion coefficient of human brain tumors at mr imaging. *Radiology* 235:985–991
- Lu S, Ahn D, Johnson G, Cha S (2003) Peritumoral diffusion tensor imaging of high- grade gliomas and metastatic brain tumors. *AJNR Am J Neuroradiol* 24:937–941
- Law M, Cha S, Knopp EA, Johnson G, Arnett J, Litt AW (2002) High-grade gliomas and solitary metastases: differentiation by using perfusion and proton spectroscopic MR imaging. *Radiology* 222:715–721
- Server A, Orheim TE, Graff BA, Josefsen R, Kumar T, Nakstad PH (2011) Diagnostic examination performance by using microvascular leakage, cerebral blood volume, and blood flow derived from 3-t dynamic susceptibility-weighted contrast- enhanced perfusion mr imaging in the differentiation of glioblastoma multiforme and brain metastasis. *Neuroradiology* 53:319–330
- Svolos P, Tsolaki E, Kapsalaki E et al (2013) Investigating brain tumor differentiation with diffusion and perfusion metrics at 3T MRI using pattern recognition techniques. *Magn Reson Imaging* 31(9):1567–1577
- Tsougos I, Svolos P, Kousi E et al (2012) Differentiation of glioblastoma multiforme from metastatic brain tumor using proton magnetic resonance spectroscopy, diffusion and perfusion metrics at 3 T. *Cancer Imaging* 12:423–436
- Griswold MA, Jakob PM, Heidemann RM, Nittka M, Jellus V, Wang J et al (2002) Generalized autocalibrating partially parallel acquisitions (grappa). *Magn Reson Med* 47:1202–1210
- Song HK, Dougherty L (2000) K-space weighted image contrast (KWIC) for contrast manipulation in projection reconstruction MRI. *Magn Reson Med* 44:825–832
- Cheng HL, Wright GA (2006) Rapid high-resolution t(1) mapping by variable flip angles: accurate and precise measurements in the presence of radiofrequency field inhomogeneity. *Magn Reson Med* 55:566–574
- Paulson ES, Schmainda KM (2008) Comparison of dynamic susceptibility-weighted contrast-enhanced mr methods: recommendations for measuring relative cerebral blood volume in brain tumors. *Radiology* 249:601–613
- Patlak CS, Blasberg RG (1985) Graphical evaluation of blood-to-brain transfer constants from multiple-time uptake data. Generalizations. *J Cereb Blood Flow Metab* 5:584–590
- Wu O, Ostergaard L, Weisskoff RM, Benner T, Rosen BR, Sorensen AG (2003) Tracer arrival timing-insensitive technique for estimating flow in mr perfusion-weighted imaging using singular value decomposition with a block-circulant deconvolution matrix. *Magn Reson Med* 50:164–174
- Basser PJ, Pierpaoli C (1998) A simplified method to measure the diffusion tensor from seven MR images. *Magn Reson Med* 39:928–934
- Haker S, Wells WM III, Warfield SK, Talos IF, Bhagwat JG, Goldberg-Zimring D et al (2005) Combining classifiers using their receiver operating characteristics and maximum likelihood estimation. *Med Image Comput Comput Assist Interv* 8:506–514
- Rees JH, Smirniotopoulos JG, Jones RV, Wong K (1996) Glioblastoma multiforme: radiologic-pathologic correlation. *Radiographics* 16:1413–1438
- Long DM (1979) Capillary ultrastructure in human metastatic brain tumors. *J Neurosurg* 51:53–58
- Kremer S, Grand S, Remy C, Esteve F, Lefournier V, Pasquier B et al (2002) Cerebral blood volume mapping by MR imaging in the initial evaluation of brain tumors. *J Neuroradiol* 29:105–113
- Cho SK, Na DG, Ryoo JW et al (2002) Perfusion MR imaging: clinical utility for the differential diagnosis of various brain tumors. *Korean J Radiol* 3:171–179
- Wang S, Kim S, Chawla S, Wolf RL, Knipp DE, Vossough A et al (2011) Differentiation between glioblastomas, solitary brain metastases, and primary cerebral lymphomas using diffusion tensor and dynamic susceptibility contrast-enhanced mr imaging. *AJNR Am J Neuroradiol* 32:507–514
- Lu S, Ahn D, Johnson G, Law M, Zagzag D, Grossman RI (2004) Diffusion-tensor mr imaging of intracranial neoplasia and associated peritumoral edema: introduction of the tumor infiltration index. *Radiology* 232:221–228
- Beaulieu C (2002) The basis of anisotropic water diffusion in the nervous system - a technical review. *NMR Biomed* 15:435–455
- Kinoshita M, Hashimoto N, Goto T, Kagawa N, Kishima H, Izumoto S et al (2008) Fractional anisotropy and tumor cell density of the tumor core show positive correlation in diffusion tensor magnetic resonance imaging of malignant brain tumors. *NeuroImage* 43:29–35
- Tsuchiya K, Fujikawa A, Nakajima M, Honya K (2005) Differentiation between solitary brain metastasis and high-grade glioma by diffusion tensor imaging. *Br J Radiol* 78:533–537
- Morita K, Matsuzawa H, Fujii Y, Tanaka R, Kwee IL, Nakada T (2005) Diffusion tensor analysis of peritumoral edema using lambda chart analysis indicative of the heterogeneity of the microstructure within edema. *J Neurosurg* 102:336–341
- McDonald DM, Baluk P (2002) Significance of blood vessel leakiness in cancer. *Cancer Res* 62:5381–5385
- Law M, Yang S, Babb JS, Knopp EA, Golfinos JG, Zagzag D et al (2004) Comparison of cerebral blood volume and vascular permeability from dynamic susceptibility contrast-enhanced perfusion mr imaging with glioma grade. *AJNR Am J Neuroradiol* 25:746–755
- Tofts PS, Brix G, Buckley DL, Evelhoch JL, Henderson E, Knopp MV et al (1999) Estimating kinetic parameters from dynamic contrast-enhanced t(1)-weighted MRI of a diffusable tracer: standardized quantities and symbols. *J Magn Reson Imaging* 10:223–232